Allocation of Gear Tolerances to Minimize Gearbox Noise Variability

Nicolas Driot, Emmanuel Rigaud, Jean Sabot, Joël Perret-Liaudet

Allocation of gear tolerances to minimize gearbox noise variability

N. Driot, E. Rigaud, J. Sabot and J. Perret-Liaudet

Laboratoire de Tribologie et Dynamique des Systèmes, UMR 5513, Ecole Centrale de Lyon

F69131 Ecully, France.

Summary

We consider a gearbox fitted out with a single helical gear and a housing with only one elastic face which radiates noise. For a gearbox manufactured in large number, a high noise level variability can result from variability of geometry faults induced by tolerances on each gear design parameters. In this paper, this noise variability is assumed to be induced by only tolerances on two gear design parameters : profile and helix angle.

Two main issues are addressed here : the first goal is to rank the influences of each geometrical parameter and to analyze their interaction on the total radiated sound power with a full factorial experiments and a variance analysis. The second issue consists of an estimation of the mean value and the standard deviation for noise level using a modified Taguchi's method.

For two quality classes of the gear, the obtained results reveal a predominance of helix angle error on the variability of the radiated sound power. Furthermore, interaction between the two studied parameters has been demonstrated.

1. Introduction

Gears generally constitute the best technological choice to transmit a motion of rotation under a high engine torque. Indeed, this kind of mechanism presents a high efficiency and leads to the weakest disturbance of input-output law (transmission error).

This transmission error is the main source of vibratory and acoustic nuisances [1-8] which designers and builders of gearboxes wish to reduce. It has been the subject of numerous theoretical and experimental studies. Considering the numerous parameters which govern these nuisances and considering the geometrical complexity of a gearbox, it is still difficult to model and to solve both vibratory and acoustic problems. Only few studies relative to acoustic behaviour of simplified gearboxes have been done [9-12].

Besides, for identical gearboxes manufactured in large number, the problem to consider is the high variability of the transmission error which leads to acoustic nuisances dispersion. The transmission error variability induced by manufacturing variance on gear design parameters and on profile modification has been studied [13, 14, 15]. However, the influence of geometry faults was not investigated and the dynamic and acoustic responses were not considered.

It is common to observe dispersion of radiated noise being able to reach more than 10 decibels for manual car gearboxes. The sources of this dispersion are numerous but they result mainly from geometry faults authorized by designers who introduce necessary tolerances on the nominal dimensions of gears and on all the surrounding mechanical components (shafts, bearings, housing). The set of tolerances values on the different geometrical gear characteristics define a "quality class" which strongly governs the manufacturing cost, so that, reducing all the tolerances in order to reduce acoustic nuisances and their dispersion would not be economically viable on products manufactured in large number.

So, theoretical, numerical or experimental searches owing to reduce acoustic nuisances and their dispersion must be based on the selection of some influential nominal characteristics and then, on the intervention on tolerances associated to these characteristics. This study presents numerical simulations dealing with the vibratory and acoustic dispersion of a typical transmission fitted out with a single helical gear, two shafts, four bearings and a steel housing.

Among all the possible geometry faults, we consider only the profile error and helix angle error. They are characterized respectively by a distance between the real profile of teeth and the theoretical profile and by a distance between the real helix angle and the theoretical helix angle. These two types of error have a sensitive influence on the noise level radiated by a

gearbox [2, 6, 8, 16]. For a constant operating speed, the spectrum of the radiated noise led by these errors is characterized by rays at the meshing frequency and its harmonics [3, 5, 8].

For several quality classes of a gear, the objective of this work is :

- to organize into a hierarchy the influence of the two retained errors on the radiated noise,
- to reveal the possible interaction among them and,
- to predict acoustic dispersion (mean value and standard deviation of the sound power) induced by the introduction of tolerances defined from every selected quality class.

The first part of this paper concerns the description of the retained typical gearbox.

The second part describes methods used for :

- computation of the static transmission error under load (source of vibratory excitation),
- computation of the vibratory response of the housing and,
- computation of the noise radiated by the housing.

The third part concerns the analysis of the dispersion of the noise radiated by the transmission for two quality classes of the gear. In a first stage, we present method and statistical tools which were retained to characterize the dispersion of the radiated noise and, in a last stage, we present and we analyze the set of results obtained from numerous numerical simulations.

2. Description of the gearbox

The gearbox retained is fitted out with a single helical gear. Each shaft is mounted between two tapered roller bearings. The steel housing (650x420x150 mm) is of the right-angled parallelepiped form made up of five 40 mm thick faces (frame) and one 6 mm thin face (450x300 mm) fixed to the frame (Figure 1 and Figure 2). This thin plate holds up two bearings supporting respectively the input and the output shafts.

This geometry was chosen so that the thin elastic face is the main source of acoustic radiation of the gearbox for low frequencies. This property leads to a large reduction of the computation time associated to the radiated noise.

This configuration of gearbox was defined and built by the TRANSSIL club which groups academics and french manufacturers together. It is installed on a test bench (Figure 3) at the Centre Technique des Industries Mécaniques (CETIM) in Senlis (France).

The main characteristics of the gear provided in Table 1 are similar to those of a gear used in car gearboxes.

3. Method of computation of the radiated sound power

To be able to analyze the statistical dispersion of the noise radiated by the gearbox, it is necessary to compute sound power radiated by its housing for several values of the profile and helix angle errors. This computation is made in three steps :

- computation of the static transmission error under load (source of vibratory excitation of the gearbox),
- computation of the vibratory response of the housing and,
- computation of the sound power radiated by the housing.

All these stages require the implementation of modelling using the finite element method and the boundary element method.

3.1 Computation of the static transmission error under load

The method used is described in detail in [17, 18]. It allows to compute static transmission error of the helical gear from its geometrical characteristics, from geometry faults and from input torque.

The computation of the static transmission error requires estimation of the loaded teeth deflections, estimation of the hertzian deformations and computation of the matrix equation which governs static equilibrium of the gear pair, for a set of successive positions of the driving wheel.

A 3D finite element modelling has been developed for each toothed wheel. A normal unitary load is applied on each node of the tooth flank. For each loaded position, the normal deflections of all nodes are computed. It allows to build the compliance matrix $\underline{\underline{H}}^{u,F}(\omega=0)$ associated with nodes of the tooth flanks. This procedure is successively applied to the pinion and the gear.

Static transmission error is expressed as a linear displacement δ along the line of action. δ is calculated for a set of successive rotational position θ of the driving wheel, in order to evaluate its time evolution. For each value of θ, a kinematic analysis of gear mesh allows to determine the location of contact line for each loaded tooth pair. The non linear matrix equation which governs static equilibrium of the gear can be written as follows :

$$\underline{\underline{H_c}}^{u,F}(\omega=0).\underline{F} = \underline{I}\,\delta(\theta) - \underline{e} - \underline{Hertz}(\underline{F}) \qquad (1)$$

$\underline{\underline{H_c}}^{u,F}(\omega=0)$ is the compliance matrix related to the nodes of contact lines. Coefficients of this matrix are combination of coefficients of the compliance matrix $\underline{\underline{H}}^{u,F}(\omega=0)$ of each toothed wheel previously computed. In equation (1), $\delta(\theta)$ corresponds to the displacement of the gear related to the pinion. This displacement is identical for the whole nodes of contact lines. $\underline{F}$ is the load vector induced by the input torque. $\underline{I}$ is the identity vector and $\underline{e}$ is the vector corresponding to the initial distance from the gear surface to the pinion surface. It is calculated from tooth surface modifications and manufacturing errors. $\underline{Hertz}$ is the non linear hertzian deformation vector calculated for each loaded tooth pair from Hertz theory.

System (1) is solved by an iterative process which allows to compute the final distribution of the load and the value of the static transmission error $\delta(\theta)$. This is performed for every discretized rotational position of the driving wheel.

The meshing stiffness is then defined by linearizing the static transmission error under load around the static equilibrium position :

$$K(F_s,\theta) = \frac{\partial(F_s)}{\partial\left[\delta(F_s,\theta)\right]} \qquad (2)$$

For a gear without geometry faults and for a low rotation speed, the time evolutions of the static transmission error and the meshing stiffness are periodic functions, fundamental frequency of which is equal to the meshing frequency f_{mesh}.

3.2 Computation of the vibratory response of the housing

The computation of the vibratory response of the gearbox induced by the static transmission error under load requires a finite element modelling of all its components i.e. gear, shafts, bearings and housing. The modelling is described in detail in [17, 19]. From this modelling, a modal analysis of the complete transmission can be done, considering the mean value of meshing stiffness.

The computation of the vibratory response is more delicate. Indeed, using time integration schemes to solve the parametric matrix equation with periodic coefficients which governs forced vibrations of the gearbox has some disadvantages. The consideration of excitation with both low frequencies (rotation frequencies of shafts) and high frequencies (meshing frequency and its harmonics) can increase drastically computation time, especially for systems with large number of degrees of freedom.

To by-pass this difficulty, we used a Spectral and Iterative Method [20] which allows to solve the large system of differential equations with periodic coefficients with reasonable computation times. This method is based on a spectral description of the meshing stiffness fluctuation and of the external force vector induced by static transmission error.

Assuming there is no loss of contact between sets of loaded tooth pair and assuming that the dynamic mesh load remains weak enough in front of static load induced by the input torque, the mean value of the meshing stiffness is not affected by the dynamic response of the transmission. Vibratory response of the modelled geared is then governed by the following system of linear differential equations with periodic coefficients :

$$\underline{\underline{M}}\,\ddot{\underline{X}}+\underline{\underline{C}}\,\dot{\underline{X}}+\underline{\underline{K}}\,\underline{X}+k(t)\underline{\underline{D}}\,\underline{X}=\underline{F}(t)+\underline{E}(t) \qquad (3)$$

In this equation, vector $\underline{X}(t)$ is the vibratory response of the gearbox, the superscript dot represents differentiation with respect to the time t. $\underline{\underline{M}}$ and $\underline{\underline{K}}$ are the classical mass and stiffness matrices provided by the finite element method. Elastic coupling between toothed wheels is introduced by k(t) which represents the periodic meshing stiffness variation. Matrix $\underline{\underline{D}}$ is derived from geometric characteristics of the gear. Matrix $\underline{\underline{C}}$ represents damping which is introduced later into every modal equation from using an equivalent viscous damping ratio for each mode. Finally, $\underline{F}(t)$ and $\underline{E}(t)$ are equivalent force vectors associated to possible external and internal excitations. In the modal base deducted from the time-invariant homogeneous counterpart equation (periodic stiffness is then replaced by its mean value), matrix equation governing vibratory response of the gearbox becomes :

$$\underline{\underline{m}}\,\ddot{\underline{q}}+\underline{\underline{c}}\,\dot{\underline{q}}+\underline{\underline{k}}\,\underline{q}+g(t)\underline{\underline{d}}\,\underline{q}=\underline{s}(t) \qquad (4)$$

In this equation, $\underline{\underline{m}}$, $\underline{\underline{c}}$ and $\underline{\underline{k}}$ are the usual modal mass, damping and stiffness diagonal matrix, $\underline{q}$ is the modal coordinates vector, $\underline{s}(t)$ is the modal force vector, and $\underline{\underline{d}}$ is the non diagonal matrix, introduced by the parametric excitation, which couples up the equations of motion.

The Spectral and Iterative Method directly gives complex spectrum of the vibratory response for each degree of freedom of the modelled gearbox. Forced responses of gear, shafts and housing are computed simultaneously. The computation time associated with this method is about 100 times shorter than that associated with classical numerical time integration schemes.

3.3 Computation of the radiated sound power

For the transmission configuration described above, the thin face of the housing is the main source of sound radiation. Then, the acoustic problem can be solved using a classical formulation, that is to say the integral direct baffled (infinite rigid plane) method coupled with the boundary element method for the description of vibrating surface. The fluid surrounding the studied gearbox is assumed to be air so that we can neglect the fluid-structure interactions. The use of this integral formulation only needs to know the normal velocity of the vibrating face S to compute the acoustic pressure P everywhere inside or outside the structure. Then, for a point Q located on the face and for harmonic excitation, the pressure P is given by the Rayleigh integral :

$$\frac{1}{4}P(Q;\omega)=i\omega\rho_0\iint_S \dot{U}(N;\omega)\,G_0(Q,N;\omega)\,dS \qquad (5)$$

where :

$$G_o(Q,N;\omega) = \exp\left(-i\underline{k}.\underline{R}(Q,N)\right)\Big/ 4\pi R(Q,N) \text{ and } R(Q,N) = \left\|\underline{Q}-\underline{N}\right\| \qquad (6)$$

$\dot{U}(N;\omega)$ is the normal velocity at N point on the surface and ρ_0 is the fluid density.

The numerical implementation of this equation can be explained in three steps :

- The first one is the discretization of the vibrating face with boundary elements. For this step, we keep the same mesh as the one used to compute the vibratory response. Then, the nodal velocity values are those computed in the section 3.2. The normal velocity on one element point is computed with the nodal values of the same element and with the shape functions. This step is referred as a collocation scheme.

- The second step consists on the numerical integration of the discretized right-hand side of equation (5). The retained method is a simple gaussian quadrature method for which it is possible to choose the number of quadrature points. We retain 2 points.

- The last step is the solving of the linear matrix system obtained with the two first steps.

The solution provides the nodal pressure values for the whole nodes on the vibrating surface without fluid-structure interaction.

All this steps are implemented by Sysnoise® vibroacoustic software.

For an accurate study of acoustic radiation problem, the largest dimension L of boundary elements is imposed by a well known condition : 6L per acoustic wavelenght. That is why most studies use a different mesh for structural and acoustic behaviour. We keep the same

mesh because the maximal frequency excitation is close to 1500 Hz. Indeed, we retain only five rays for the description of the vibratory response spectrum and the highest frequency is equal to $f=5f_{mesh}$. This frequency is itself close to the maximal authorized acoustic frequency.

The results accuracy is very sensitive to the order of collocation scheme. The boundary elements contain 3 and 4 nodes so that the collocation scheme is order 1.

At this time, the available results allow to compute the radiated sound power. For an harmonic excitation with frequency ω the radiated sound power is given by :

$$\Pi_{ac}(\omega) = \frac{1}{2}\sum_{m}\iint_{S_m} \mathrm{Re}\left(P_m(\omega)\dot{U}_m^*(\omega)\right) dS_m \qquad (7)$$

where m represents the element of surface S_m. The pressure values P_m and the normal velocity $\dot{U}_m$ on this surface element are extrapolated from their nodal values and from the shape functions.

For an harmonic excitation, the sound power level is :

$$\Pi_{ac}(\mathrm{dB}) = 10\log(\Pi_{ac}/\Pi_{ac}^{ref}) \text{ with } \Pi_{ac}^{ref} = 10^{-12}\,\mathrm{Watts} \qquad (8)$$

This calculation leads to the total sound power level defined by the following relation :

$$\Pi_{actot}(\mathrm{dB}) = 10\log(\sum_{\omega} 10^{\Pi_{ac}(\mathrm{dB})/10}) \qquad (9)$$

In order to calculate the radiation efficiency of the structure, it is necessary to know the injected power in the structure. This injected power is related to the spatial average $< \overline{V^2(\omega)} >$ of the mean time square normal velocity by the following relationship :

$$W_{inj}(\omega) = \rho_0 c_0 S < \overline{V^2(\omega)} > \qquad (10)$$

The results being presented in section 5 deal with a quadratic velocity level defined by :

$$L_{quad}(\mathrm{dB}) = 10\log\left(< \overline{V^2(\omega)} > / 2.5\cdot 10^{-15}\right) \qquad (11)$$

Then, the radiation efficiency is deduced from the following expression :

$$\sigma(\omega) = \frac{\Pi_{ac}(\omega)}{W_{inj}(\omega)} \qquad (12)$$

4. Calculation of the radiated noise variability : statistical tools

Two issues are addressed here : we want to perform an analysis of the influence of each geometric faults and their interaction and secondly, we want to predict the first two moments of the noise distribution. The two retained methods perform a factorial experiments.

4.1 Influence analysis method

Several methods can be used to organize into a hierarchy the influence of geometry faults on the dispersion. For example, it would be possible to lead a fault by fault traditional analysis or a Monte-Carlo simulation. However, the first one can't take into account interactions between parameters and the second one requires a very large number of the total sound power computations.

The full factorial experiments method or the fractional factorial experiments method allows to take into account interactions between parameters with reasonable response computations. That is why we have retained this method for our study.

The factorial experiments method requires the building of a linear matrix regression model of the response associated with an appropriate orthogonal array. Responses are computed for each event of the orthogonal array and the model coefficients are calculated [21]. Then, an analysis of variance using the matrix regression model coefficients is implemented in order to estimate variances inferred by every geometry fault and by interaction. The more influent a fault is, the higher inferred variance is.

For two geometry faults (P, H) with interaction, the linear matrix regression model can be written as follows :

$$Y = M + {}^{t}\underline{E}_{P}\underline{P} + {}^{t}\underline{E}_{H}\underline{H} + {}^{t}\underline{PI}_{P,H}\underline{H} \qquad (13)$$

where the matrix coefficients are equal to $E_{Pi}=M_{Pi}-M$, $I_{Pi,Hj}=M_{Pi,Hj}-M-E_{PI}-E_{Hj}$, with i, j representing the different geometry faults levels of the orthogonal array.

M is the mean value of the responses, M_{Pi} is the mean value of the responses when P=i, $M_{Pi,Hj}$ is the mean value of the responses when P=i, H=j. Components of vectors $\underline{P}$ and $\underline{H}$ are equal to 0 or 1 according to the levels of factors P (profile error) and H (helix angle error).

The choice of the orthogonal array depends explicitly on the model one wishes to study [22, 23]. In order to take into account weak non-linear effects, we choose to represent each factor by 3 levels, so that i, j=1, 2, 3 in equation (13).

Furthermore, we want to reduce the number of sound power evaluations because of time cost associated with calculation procedure. We propose to use the same orthogonal array for both parameter influences analysis and statistical moments estimations. The factorial experiments which has been retained is the orthogonal array called $L_9(3^4)$ by Taguchi [22, 23]. The order of numerical experiments is illustrated in Table 2.

The $L_9(3^4)$ orthogonal array allows to study four factors with three levels per factor and without interactions. It also allows to study two factors with three levels and with interaction. This last case corresponds to our gearbox which has only two geometry faults. The profile error is affected in column 1, the helix angle error is affected in column 2. Columns 3 and 4 are used to analyze interaction between the two faults (Table 2).

For each of the 3 levels, the corresponding value of the geometry fault to be introduced in the orthogonal array is not subjected to any mathematical criterion. Nevertheless, the tolerance range induced by the choice of a quality class must be explored with three different values for each geometry fault (the tolerance range is about ±10 µm).

On the other hand, the method to calculate dispersion induced by the two faults imposes a particular value attributed to every level. This method is described below. So, our choice is related to this condition.

It must be specified that the analysis of variance compares a tabulated value with the ratio between the variance of the factor and a residual variance. It is the Snedecor test [21]. This test allows to interpret the influence of a factor. In our case, it is impossible to calculate a residual variance because there is no more degree of freedom to evaluate the residual variance. So, we can only compare variances inferred by each geometry fault but we can not include the variance of the interaction in this comparison. Indeed, tabulated value given with Snedecor's table for an interaction is not the same than the tabulated value given for faults. So that, in order to reveal interaction, we used the graphic technique proposed in [24]. This method is frequently used in analysis of factorial experiments.

Once the geometry faults have been organized into a hierarchy, the method retained for the analysis of the acoustic dispersion is then described.

4.2 Moments estimation method

Concerning the $L_9(3^4)$ orthogonal array, the choice of the level value of every fault depends on the method used to calculate the statistical moments of the radiated sound power.

This method is proposed by D'Errico [25]. It allows to characterize statistical distribution of a function with several random variables having known distribution, from the calculation of its moments. It is based on the use of a full factorial experiments. The value v of a level depends on the statistical distribution of factors.

The orthogonal array $L_9(3^4)$ is a full factorial experiments with three levels for two factors because it contains nine experiments. For products manufactured in large numbers, one assumes that the distributions of the geometry fault values are normal distributions. According to the D'Errico's method, the level values v are :

Level 1: $v = \mu_i - \sigma_i.\sqrt{3}$ with weight 1/6,

Level 2: $v = \mu_i$ with weight 4/6,

Level 3: $v = \mu_i + \sigma_i.\sqrt{3}$ with weight 1/6.

μ_i represents mean value of every factor and σ_i represents its standard deviation. Figure 4 illustrates value associated to each of the 3 levels.

For the gearbox studied, the mean value of every fault is zero. The corresponding value of the total sound power is taken as the nominal reference.

Standard deviation of every geometry fault is unknown but the tolerance range Δ in which every fault can evolve is known. Δ depends on the quality class and on the kind of geometry fault. If one assumes that the distribution of values of the geometry fault is a normal distribution, the probability for the value to be included in $\pm 3\sigma$ is equal to 0,997. This condition implies that: $\Delta = 3\sigma$.

Table 3 gives the value of the geometry fault for each level and for a given quality class.

Sound powers (responses Y_k) are computed in $N=3^n$ combinations of geometry faults of the full factorial experiments. The first two moments of the distribution of the radiated sound power are then given by :

$$m_1 = \sum_{k=1}^{N} W_k Y_k$$
$$m_2 = \sum_{k=1}^{N} W_k (Y_k - m_1)^2 \qquad (14)$$

W_k is the product of the weights of every combination of levels. It is given in Table 2.

This statistical tolerancing method is reliable under certain conditions common to the numerical gaussian quadrature integration methods. The response function must be continuous and must present only smooth non-linear variations. In this context, the calculation of the moments of order 1 and 2 is very accurate and simple. Main handicap comes from the number of responses to estimate in the case of a function with 4 random variables (81 attempts) or more.

5. Results

All tolerances correspond to AFNOR French standard NF E 23-006. The first numerical simulations correspond to a quality class 8 for the profile error and the helix angle error (P8-H8 configuration). The tolerance ranges associated to these two geometry faults are equal respectively to ±18 µm and ±20 µm. This quality class is often used in industrial applications (gearbox, machine-tool, …).

For the whole presented results, the rotation speed of the input shaft of the gearbox is equal to 1000 rpm, the engine torque is equal to 60 Nm and the mean value of the meshing stiffness is equal to 350 N/µm.

Figure 5 displays the 9 spectra of the quadratic velocity level of the housing in the increasing order of the factorial experiments attempts. For this study, it appears to be sufficient to define the spectrum of periodic transmission error by its first 5 rays. This assumption is often done in gear dynamics. The first ray is relative to the meshing frequency f_{mesh}.

Dispersion of the quadratic velocity level can be observed for each of the 5 rays. The higher the row of a ray is, the higher the dispersion is. For the last ray, it reaches more than 25 dB.

The level of the first harmonic of the spectrum ($f=2\ f_{mesh}$) is the highest for all attempts. The reference attempt without geometry faults (attempt 1) is not always the lowest quadratic velocity level. Nevertheless, it is the lowest one for the dominant ray ($f=2\ f_{mesh}$).

Figure 6 displays the spectra of sound radiated by the housing. Results are similar to those observed for the quadratic velocity spectra. In fact, for a given frequency, the sound power level is a linear function of the quadratic velocity level.

Figure 7 displays the evolution of the radiation efficiency of the housing according to the frequency.

Figure 8 displays the total sound power level for each attempt of the factorial experiments, calculated from the spectrum of sound power. Dispersion is larger than 10 dB. Attempt 1 (reference) is the less noisy but attempt 8 is noiseless too. The noise level is low because rotation speed of the gearbox is relatively weak (1000 rpm) and it does not allow to excite some particular modes leading to high vibratory and acoustic levels in a resonant manner [18, 19].

A variance analysis is done in order to analyze the influence of each geometry fault. For that, a matrix linear model of the sound power is built for every frequency. Results are presented in Table 4. The helix angle error dominates, for all rays. So, reduction of the dispersion may certainly be obtained by a decrease of the quality class affected to helix angle, the quality class relative to profile error remaining unchanged.

It is possible to repeat this kind of variance analysis with values obtained for the total sound power. Table 5 presents corresponding results. Even there, we find that the helix angle error dominates.

Let’s consider the problem of interaction between the profile error and the helix angle error. The results obtained from the graphic technique are displayed in Figure 9. Every point corresponds to the value of the total sound power radiated for one attempt of the factorial experiments. The evolutions of the total sound power are quite different when we change the level of helix angle error. This result demonstrates clearly the importance of interaction between the two geometry faults. Finally, when the helix angle error is zero, the total sound power has very little variations.

The estimation of the acoustic dispersion due to the two geometry faults is done with the method described above. Obtained results are presented in Table 6. Average deviation is defined by the difference between mean value and reference value. Dispersion is the highest on rays 2 and 5. These rays contribute strongly to the acoustic efficiency.

Characteristics of the dispersion of the total sound power are presented in Table 7. The standard deviation of the total sound power is higher than its mean value. The noise statistical distribution is not a normal distribution so that such a result is not surprising. Most of manufactured gearboxes would radiate noise level close to the reference value. In order to analyze the meaning of this standard deviation, one can use Tchebycheff's inequality. For the P8-H8 configuration, we find the maximal probability to have a total sound power higher than 65.3 dB is equal to 4 %.

In the light of the set of obtained results, one can try to reduce acoustic dispersion by changing the quality class of the most influential fault, that is to say the helix angle error. For that, we consider a new configuration. It corresponds to quality class 8 for profile error and quality class 7 for helix angle error. For this P8-H7 configuration, the new tolerance range associated to helix angle error is equal to ±12 µm. Numerical results obtained for the spectra of quadratic velocity level are displayed in Figure 10 and those obtained for the spectra of sound power level are displayed in Figure 11.

With regard to the P8-H8 configuration, dispersion between the 9 attempts of the factorial experiments is appreciably reduced for each ray, especially for ray 1.

Table 8 presents the average deviations of the quadratic velocity level for every ray of the spectrum. The maximum of dispersion is observed for rays 2, 3 and 5. This result constitutes a second difference with regard to the P8-H8 configuration.

Figure 12 displays the total sound power level for the 9 attempts of the factorial experiments. Dispersion has strongly decreased. Reference attempt is always the less noisy.

The variance analysis of the spectra of sound power provides results presented in Table 4. The helix angle error is still more influential than the profile error, in spite of the decrease of the quality class. However, deviations of ray 2, ray 3 and ray 5 have decreased.

For the new P8-H7 configuration, results from the graphic technique used to analyze the interaction between the two geometry faults are displayed in Figure 13. The influence of the helix angle error is weaker when its level is level 1. We also notice that distance between max value and min value decreased appreciably. When helix angle error is null (level 2), sound power evolution is similar to the one corresponding to the P8-H8 configuration because values correspond to the same attempts.

The new characteristics of the acoustic dispersion are presented in Table 6. Average deviation has decreased for all rays, excepted for the third ray.

The results of the estimation of the dispersion of the total sound power are presented in Table 7. Standard deviation is lower than the mean value. This one is lower than the one obtained for the P8-H8 configuration and the maximal probability to obtain a level of noise higher than 62.2 dB is 4 %.

At last, we present results obtained for a third configuration (P7-H8 configuration) for which we can expect a decrease of the dispersion weaker than for the previous P8-H7

configuration. The tolerance range associated to the profile error is then equal to 13 µm. For this new configuration, Results are displayed in Figure 14 and in Table 7. The decrease of the dispersion is in adequacy with forecasts because results are situated between configurations P8-H8 and P8-H7. However, reduction of noise dispersion is rather weak. The maximal probability to obtain a level of noise higher than 63.2 dB is 4 %. The decrease of the tolerance associated with profile error does not appear to be a good choice to reduce appreciably acoustic dispersion.

6. Conclusion

In this study, we implemented statistical methods to describe the variability of the noise radiated by the housing of a gearbox fitted out with a single helical gear.

Among all the geometry faults of the gear being able to contribute to the variability of the radiated noise, the analysis was focused on two faults : profile error P and helix angle error H.

The ranges of variation associated to these two geometry faults corresponded to quality class 8 and quality class 7.

This method allowed to supply a statistical description of the sound power radiated by the studied transmission from a set of 27 numerical simulations (9 simulations for the P8-H8 configuration, 9 simulations for the P8-H7 configuration and 9 simulations for the P7-H8 configuration). Each numerical simulation implies the computation of the transmission error, vibratory response of the housing and radiated sound power.

Obtained results lead to the following main conclusions :

- For the P8-H8 configuration, the variability can reaches more than 25 dB for some rays of the noise spectrum,
- Interaction between the profile error and the helix angle error has been demonstrated.
- The comparison between P8-H8, P8-H7 and P7-H8 configurations demonstrates that the helix angle error has more influence on the variability of the radiated noise than the profile error.
- The reduction of the range of variation associated with helix angle error is the most effective to reduce appreciably the variability of radiated noise.

In conclusion, the implemented methodology allowed to predict qualitatively the influence of geometry faults and to predict quantitatively the statistical characteristics of the variability of the noise radiated by the housing of a gearbox. One can so intend to introduce other types

of geometry faults on the gear (eccentricity, pitch error…) to minimize level and variability of this noise. Nevertheless, the methodology used in this study is restricted to linear (or weakly non-linear) dynamic modellings of gearboxes. Under some particular operating conditions, contact losses between teeth may occur because of gear backlash. Induced dynamic behaviour of the gear pair becomes non-linear. So that, other tools should be elaborated for studying the influence of this backlash on the radiated noise variability.

7. References

[1] S. Harris : Dynamic loads on the teeth of spur gears. Proc. I. Mech. E, 1958, 172 87-112.

[2] H. Opitz : Noise of gears. Phil. Trans. of Royal Society **263** (1969) 369-380.

[3] D. Welbourn : Gears errors and their resultant noise spectra. Proc. I. Mech. E., 1970, 184 131-139.

[4] W. Mark : Analysis of the vibratory excitation of gear systems : basic theory. J. Acoust. Soc. Am. **63** (1978) 1409-1430.

[5] D. Welbourn : Fundamental knowledge of gear noise – A survey. Proc. I. Mech. E., 1979, paper C117, 09-14.

[6] J. Derek Smith : A basic approach to understanding gear noise. The MacMillan Press LDT., 1983.

[7] T. Lim and R. Singh : A review of gear housing dynamics and acoustics literature.NASA Contractor Report 185148, 1989.

[8] D. Rémond, P. Velex, J. Sabot : Comportement dynamique et acoustique des transmissions par engrenages. Synthèse bibliographique. Publication du CETIM, France, 1993.

[9] M. Kato, H. Zhou, K. Inoue, K. Shibata : Evaluation of sound power radiated from gearbox. Proc. of I. Gearing Conf., UK National Gear Metrology Laboratory, 1994, 69-74.

[10] M. Kato, H. Zhou, K. Inoue, K. Shibata, M. Yasunami : Comments on gearbox housing structure for low noise. VDI Berichte **1230** (1996), 765-777.

[11] P. Ducret, J. Sabot : Calcul du bruit rayonné par les carters des transmissions à engrenages – Méthode et applications. Acustica–Acta acustica **84** (1998), 97-107.

[12] P. Ducret : Prédiction du bruit rayonné par les carters des transmissions à engrenages. Thèse de l'Ecole Centrale de Lyon, France, 1997.

[13] S. Sundaresan, K. Ishii, D. Houser : A procedure using manufacturing variance to design gears with minimum transmission error. ASME Journal of Mechanical Design **113** (1991), 318-324.

[14] S. Sundaresan, K. Ishii, D. Houser : A robust optimization procedure with variations on design variables and constraints. ASME Advances in Design Automation **65** (1993), 379-386.

[15] J.C. Yu, K. Ishii : Design for robustness based on manufacturing variation patterns. ASME Journal of Mechanical Design **120** (1998), 196-202.

[16] K. Umezawa, T. Suzuki, H. Houjoh, K. Bagiasna : Influence of misalignment on vibration of helical gear. Proc. of the 2nd world Congress on Gearing, Paris, 1986, 615-626.

[17] E. Rigaud : Interactions entre dentures, lignes d'arbres, roulements et carter dans les transmissions par engrenages. Thèse de Doctorat de l'Ecole Centrale de Lyon, France, 1998.

[18] E. Rigaud, D. Barday : Modelling and analysis of static transmission error – Effect of wheel body deformation and interactions between adjacent teeth. Proc. of the 4th World Congress on Gearing and Power Transmission, Paris, 1999, 1961-1970.

[19] E. Rigaud, J. Sabot : Effect of elasticity of shafts, bearings, casing and couplings on the critical rotational speeds of a gearbox. VDI-Berichte **1230**, 1996, 833-845.

[20] J. Perret-Liaudet : An original method for computing the response of parametrically excited forced system. J. of Sound and Vibration, **196** (1996) 165-177.

[21] M. Pillet : Introduction aux plans d'expériences par la méthode Taguchi. Les Editions d'Organisation, France, 1994.

[22] G. Taguchi : Off-line and on-line quality control systems. Proc. of I. Conf. on Quality Control, 1978, Tokyo.

[23] G. Taguchi, S. Konishi : Orthogonals arrays and linear graphs. American Supplier Institute Press, 1987.

[24] D.M. Byrne, S. Taguchi : The Taguchi approach to parameter design. ASQC Quality Congress Transaction, Anaheim USA, 1986, 168-177.

[25] J. D'Errico, N. Zaino : Statistical tolerancing using a modification of Taguchi's method. Technometrics, **30** (1988), 397-405.

	Pinion	**Driven wheel**
Number of teeth	17	71
Base radii (mm)	23.397	97.718
Normal module (mm)	2.676	2.676
Base helix angle	24°	
Transverse pressure angle	18.877°	
Facewidth (mm)	20	
Centre distance (mm)	128	

Table 1. Main geometrical characteristics of the helical gear.

factors	**1**	**2**	**3**	**4**	Response	Weightings W_k
Attempt 8	1	1	1	1	Y_8	1/36
Attempt 7	1	2	2	2	Y_7	4/36
Attempt 9	1	3	3	3	Y_9	1/36
Attempt 2	2	1	2	3	Y_2	4/36
Attempt 1	2	2	3	1	Y_1	16/36
Attempt 3	2	3	1	2	Y_3	4/36
Attempt 5	3	1	3	2	Y_5	1/36
Attempt 4	3	2	1	3	Y_4	4/36
Attempt 6	3	3	2	1	Y_6	1/36

Table 2. $L_9(3^4)$ orthogonal array with weightings of each attempt.

Geometry fault levels	Geometry fault values
1	$0-\Delta\frac{\sqrt{3}}{3}$
2	0
3	$0+\Delta\frac{\sqrt{3}}{3}$

Table 3. Correspondence between geometry fault levels and geometry fault values.

Configuration	P8-H8		P8-H7	
Variance (Watts²)	P	H	P	H
Ray 1	$5.78\ 10^{-17}$	**$5.97\ 10^{-16}$**	$1.09\ 10^{-17}$	**$1.14\ 10^{-16}$**
Ray 2	$7.85\ 10^{-13}$	**$1.02\ 10^{-12}$**	$1.44\ 10^{-13}$	**$5.25\ 10^{-13}$**
Ray 3	$9.12\ 10^{-18}$	**$5.70\ 10^{-17}$**	$1.25\ 10^{-16}$	**$1.37\ 10^{-16}$**
Ray 4	$1.76\ 10^{-16}$	**$3.90\ 10^{-16}$**	$4.76\ 10^{-17}$	**$6.79\ 10^{-16}$**
Ray 5	$3.40\ 10^{-17}$	**$7.52\ 10^{-17}$**	$2.22\ 10^{-17}$	**$2.40\ 10^{-17}$**

Table 4. Sound power variance for each factor and for P8-H8 and P8-H7 configurations.

Variance P	$7.97\ 10^{-13}$
Variance H	$\mathbf{1.11\ 10^{-12}}$

Table 5. Total sound power variance (Watts²) for P8-H8 configuration.

Configuration	P8-H8		P8-H7	
	Mean value (dB)	Average deviation (dB)	Mean value (dB)	Average deviation (dB)
Ray 1	41.8	3	40.5	1.7
Ray 2	55.6	5.9	53.9	4.2
Ray 3	38.5	0.9	40	2.4
Ray 4	46.6	2.1	47	1.7
Ray 5	36	5	33.4	2.4

Table 6. Acoustic dispersion for P8-H8 and P8-H7 configurations.

	P8-H8	P8-H7	P7-H8
$\overline{\Pi_{actot}}$ (dB)	56.4	**55**	55.5
(Watts)	$4.35\ 10^{-07}$	$\mathbf{3.17\ 10^{-07}}$	$3.57\ 10^{-07}$
Average deviation (dB)	3.8	**2.4**	2.9
Standard deviation (Watts)	$5.85\ 10^{-07}$	$\mathbf{2.67\ 10^{-07}}$	$3.51\ 10^{-07}$

Table 7. Statistical characteristics of total sound power distributions for whole testing configurations.

	Ray 1	Ray 2	Ray 3	Ray 4	Ray 5
Average deviation (dB)	3.2	12.9	-1.6	2.9	-10.6

Table 8. Average deviation of the quadratic velocity level for P8-H7 configuration.

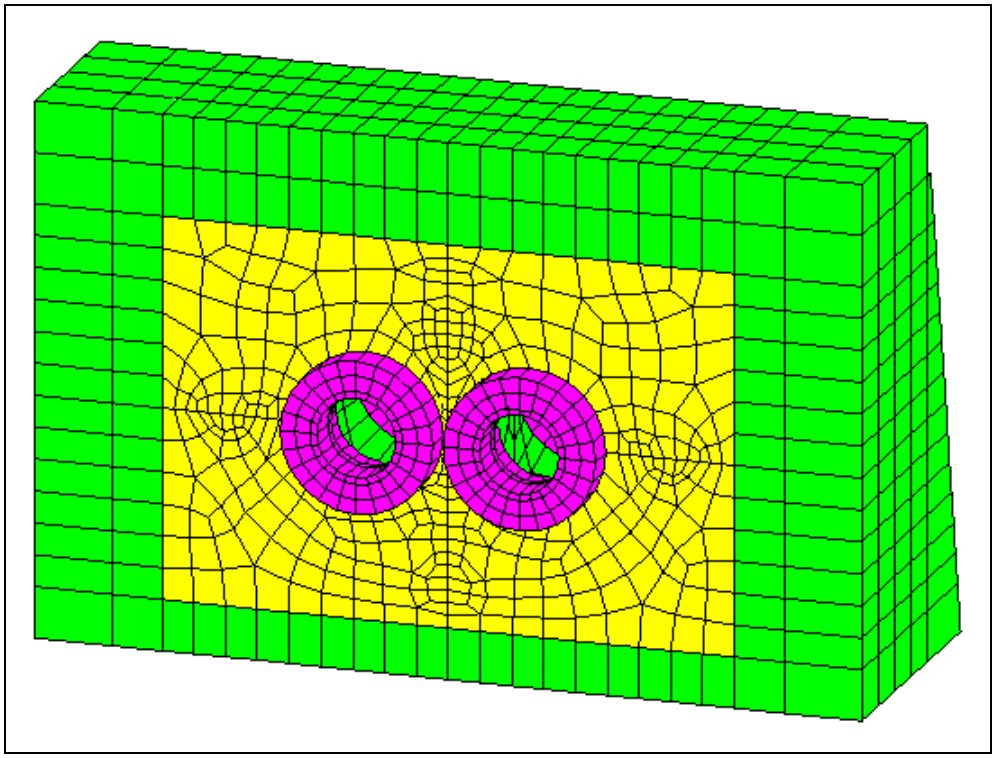

Figure 1. Finite element modelling of the housing of the studied gearbox. View of the free side.

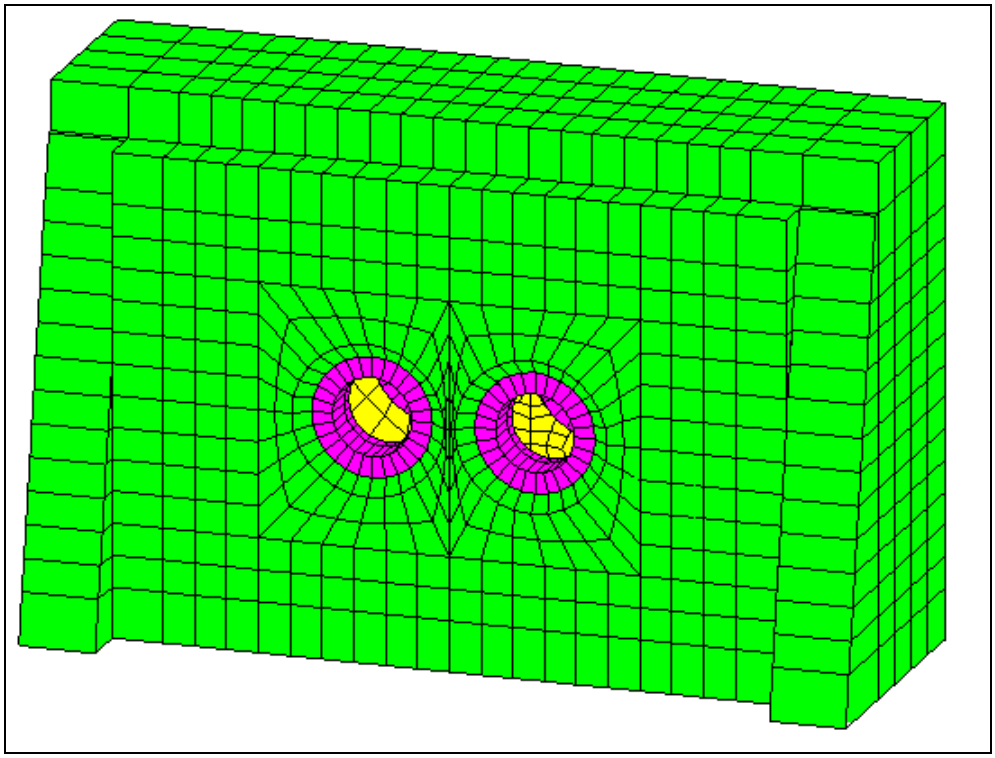

Figure 2. Finite element modelling of the housing of the studied gearbox. View of the Opposite side.

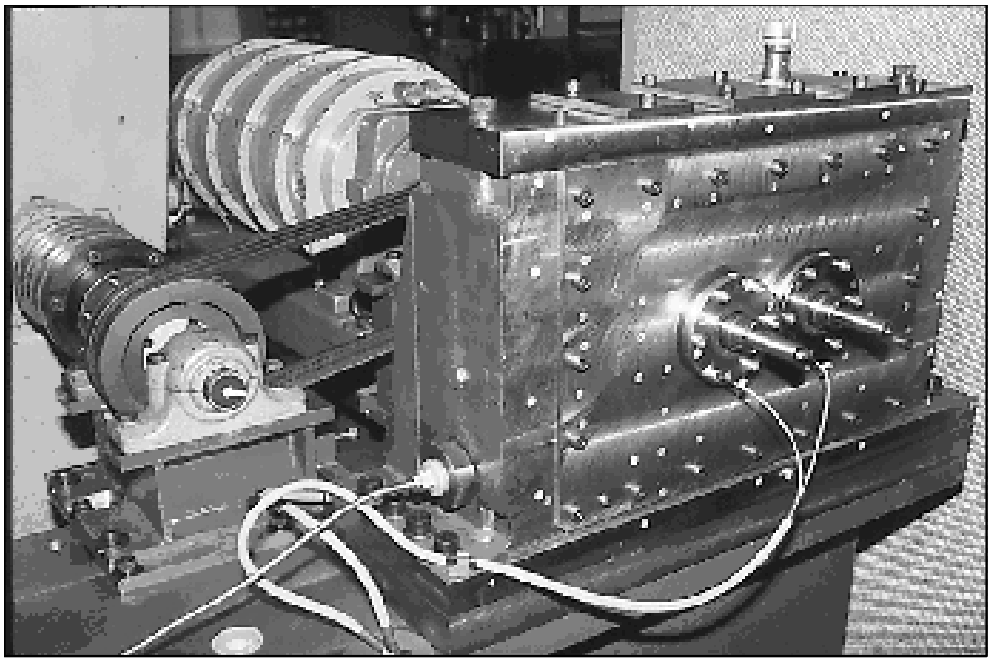

Figure 3. Test bench installed in the CETIM at Senlis, France.

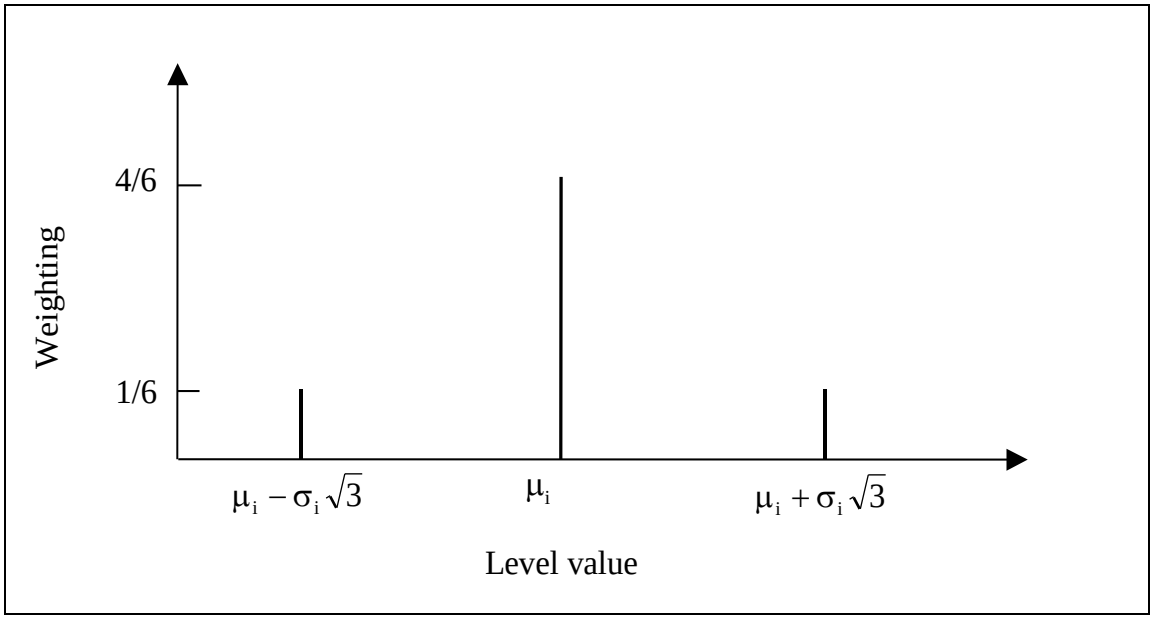

Figure 4. Selection of the three level values and associated weighting.

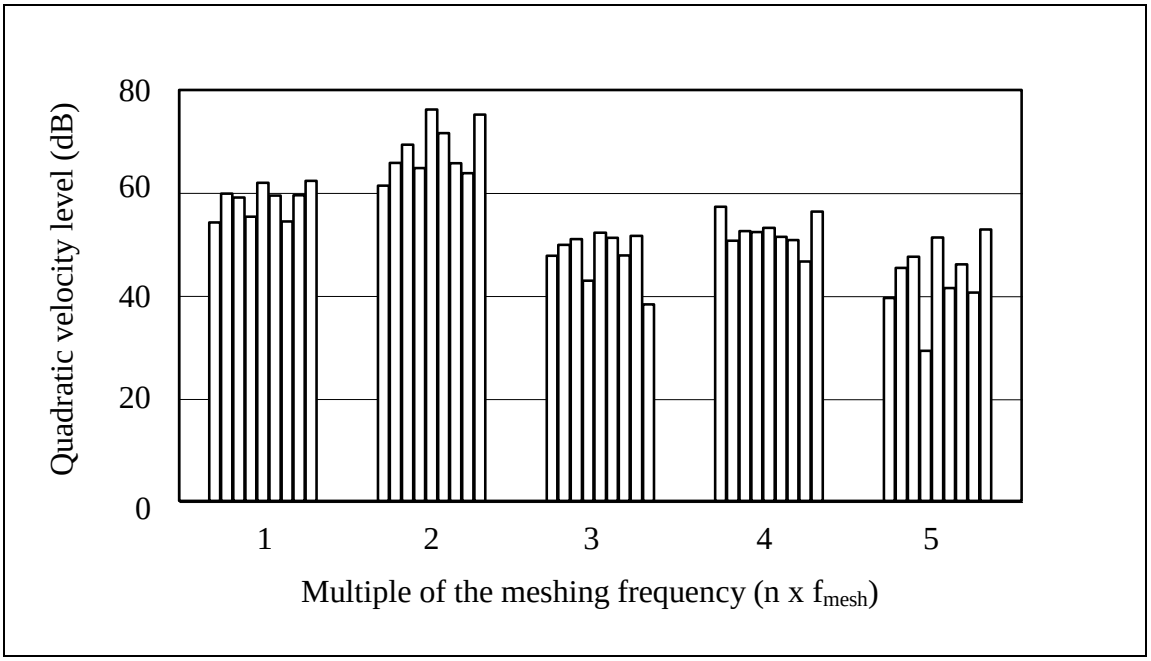

Figure 5. Spectra of the housing quadratic velocity level for the 9 numerical attempts in increasing order. P8-H8 Configuration.

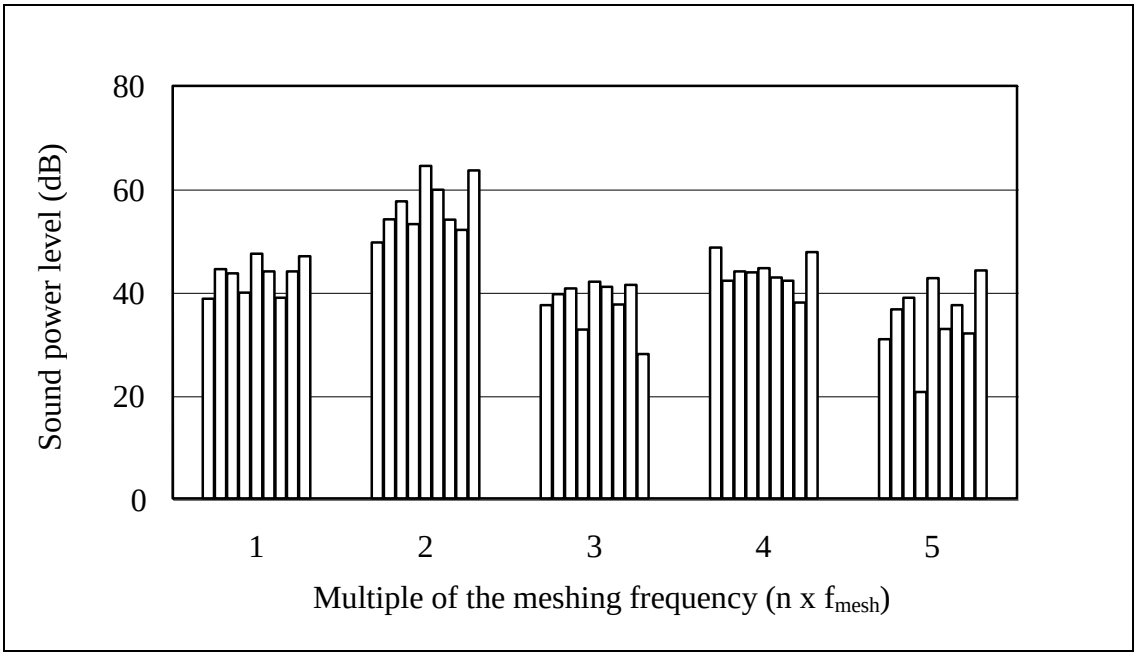

Figure 6. Spectra of the sound power level for the 9 numerical attempts in increasing order. P8-H8 Configuration.

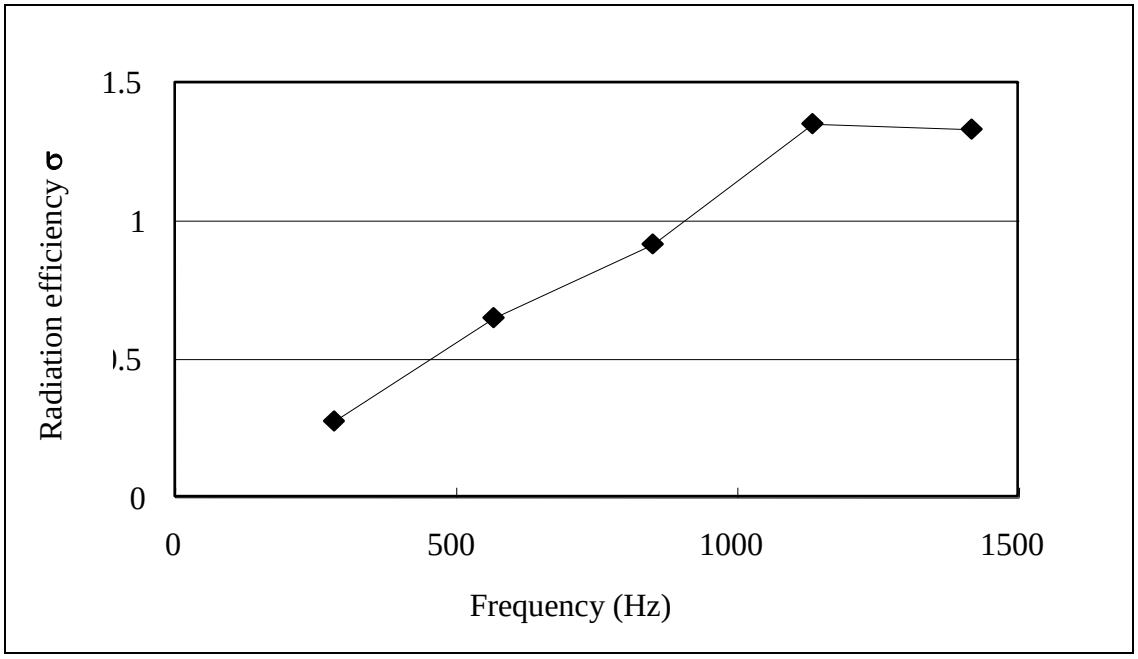

Figure 7. Frequency evolution of the housing radiation efficiency.

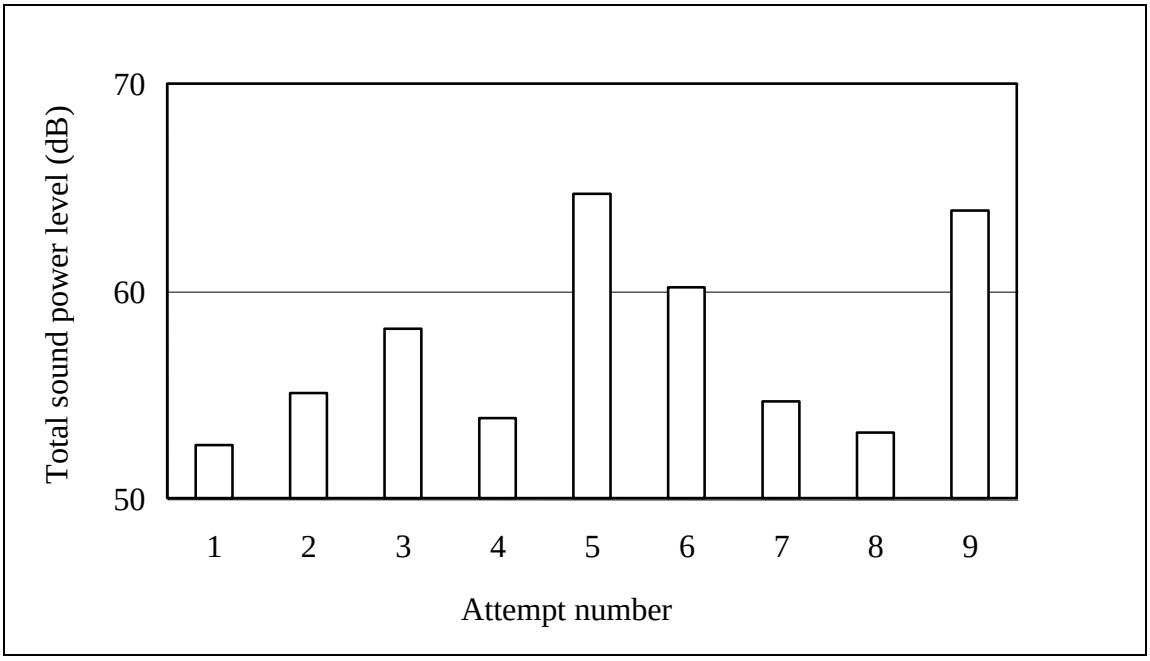

Figure 8. Total sound power level for each of 9 attempts. P8-H8 Configuration.

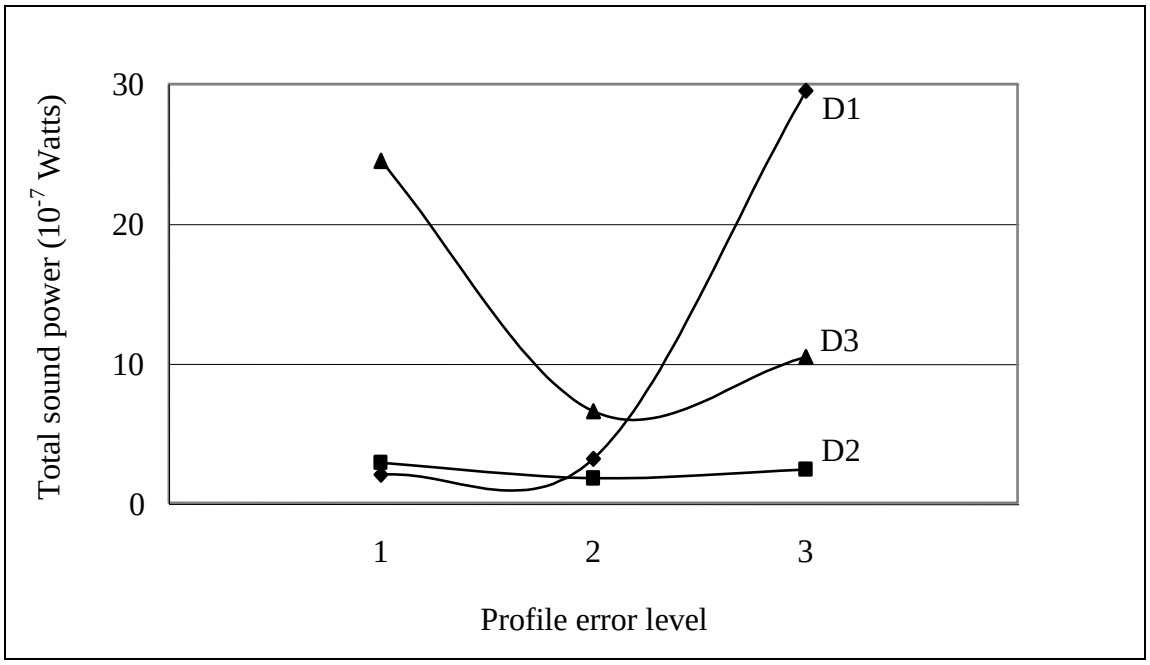

Figure 9. Interaction representation between profile error and helix angle error. P8-H8 Configuration.

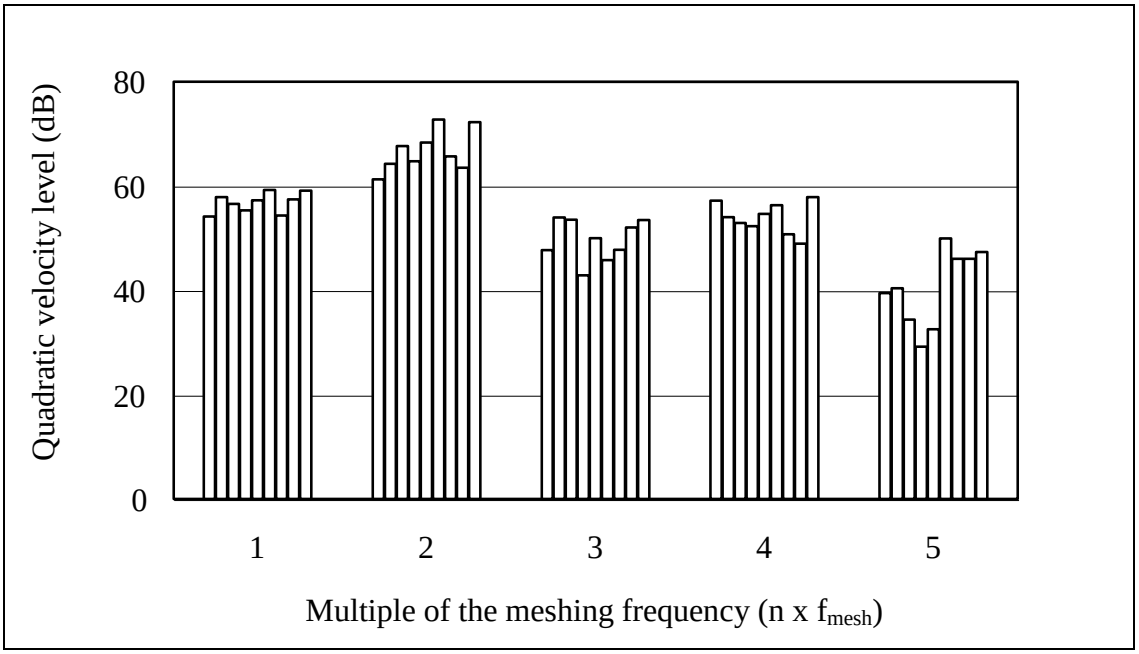

Figure 10. Spectra of the housing quadratic velocity level for the 9 numerical attempts in increasing order. P8-H7 Configuration.

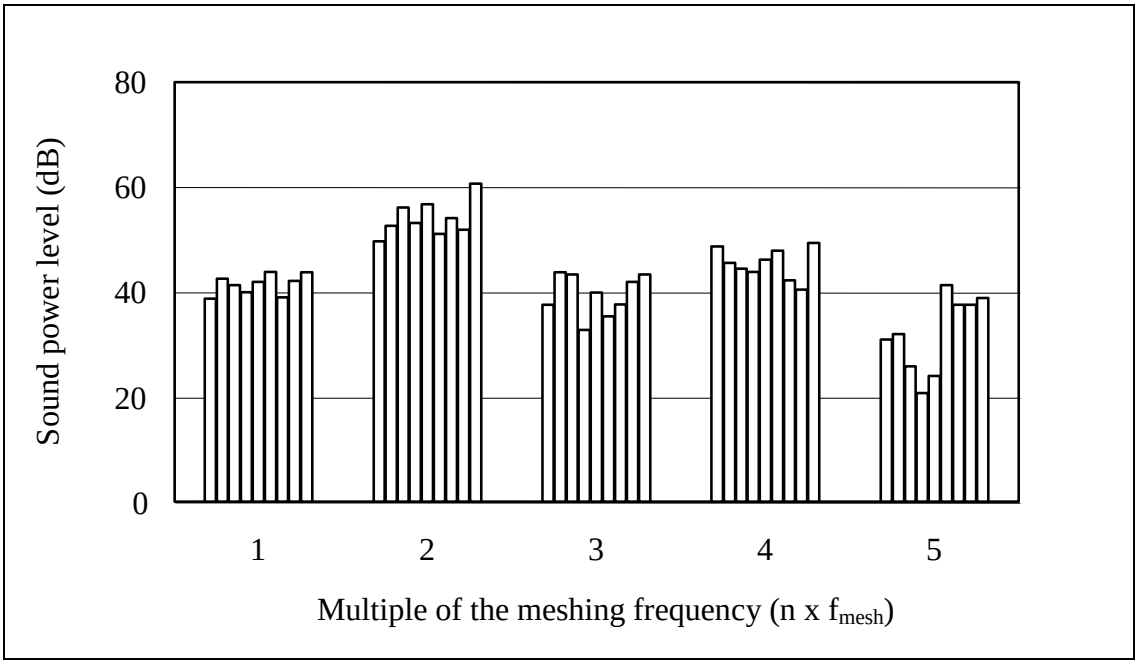

Figure 11. Spectra of the sound power level for the 9 numerical attempts in increasing order. P8-H7 Configuration.

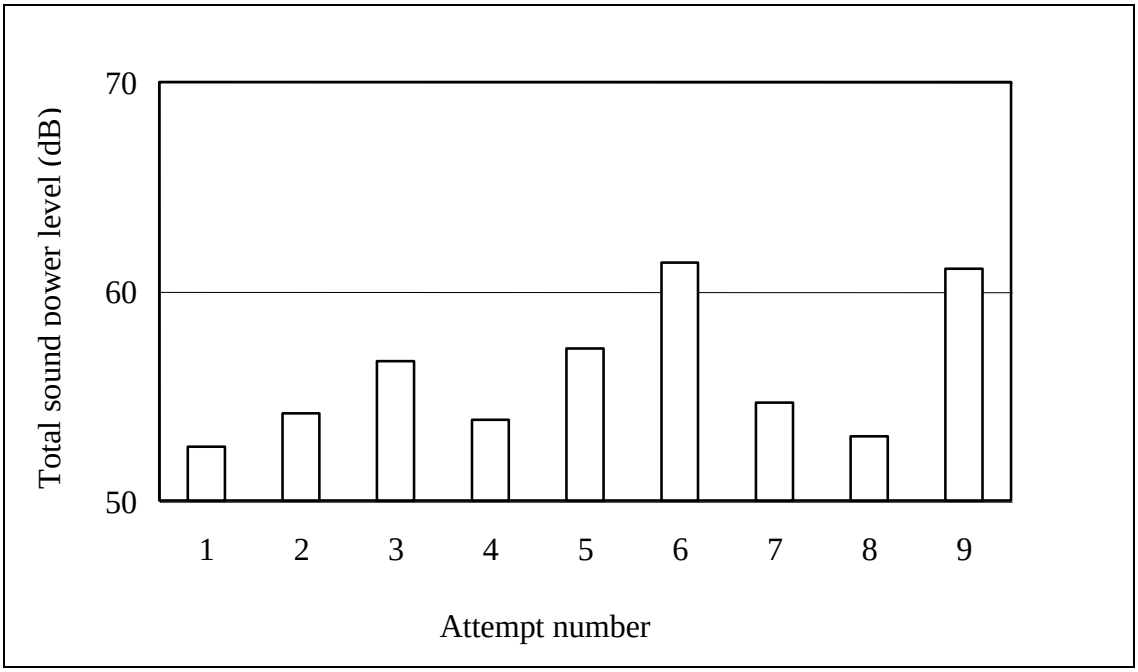

Figure 12. Total sound power level radiated by the housing for each of the 9 numerical attempts. P8-H7 Configuration.

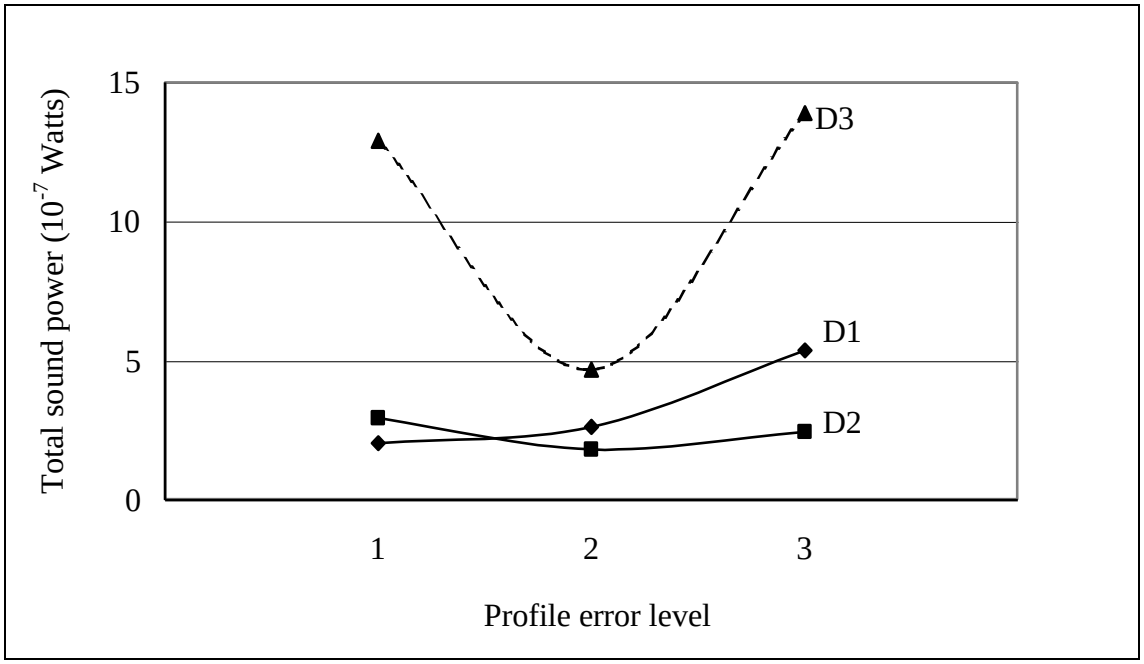

Figure 13. Interaction representation between profile error and helix angle error. P8-H7 Configuration.

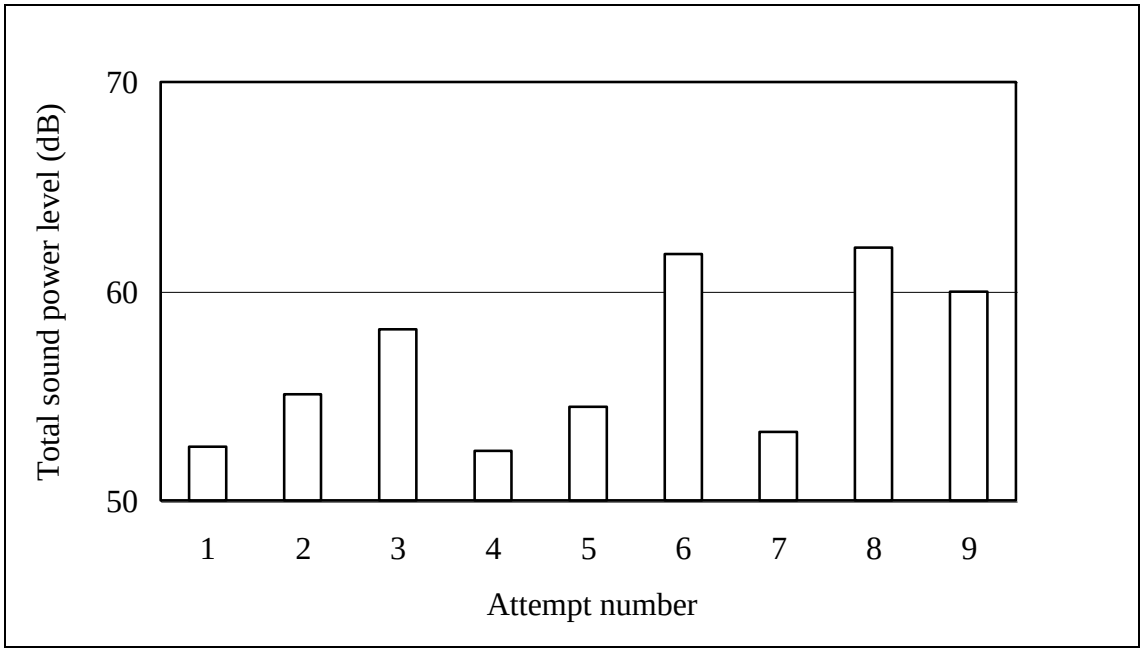

Figure 14. Total sound power level for each of the 9 numeric attempts. P7-H8 Configuration.